AJAB

Asian J Agric & Biol. 2019; Special Issue: 33-47.

Original Article

Diversity and marine sustainability of Setiu wetland: modified calcium phosphate from Tamban bones as alternative sunscreen materials

Mohd Zul Helmi Rozaini [1*], Habibah Hamzah[2], Mohd Hasmizam Razali[3], Uwaisulqarni M. Osman[3], Chia Poh Wai[3], Siti Kamilah Che Soh[3], Saidatul Radhiah Ghazali[4], Nor Hayati Ibrahim[2], Low Chen Fei[5]

[1]Institute of Marine and Biotechnology, Universiti Malaysia Terengganu, 21030 Kuala Nerus, Terengganu, MALAYSIA.
[2]Faculty of Fisheries and Food Sciences, Universiti Malaysia Terengganu, 21030 Kuala Nerus, Terengganu, MALAYSIA.
[3]Faculty of Science and Marine Environment, Universiti Malaysia Terengganu, 21030 Kuala Nerus, Terengganu, MALAYSIA.
[4]Faculty of Chemical Engineering Technology, Tati University College, 24000, Kemaman, Terengganu, MALAYSIA.
[5]Institute of Systems Biology, Universiti Kebangsaan Malaysia, 43600 Bangi, Selangor, MALAYSIA

Received:
March 10, 2019
Accepted:
November 04, 2019
Published:
December 05, 2019

**Corresponding author email:*
zulhelmi@umt.edu.my

Abstract

Fringescale sardinella or Tamban sisik bones have been discovered can be utilized as sunscreen agent in cosmeceuticals. Its flesh is the main ingredient in *keropok lekor* or fish crackers in Malaysia and the bones contained very high hydroxyapatite (HAp), ($Ca_{10}(PO_4)_6(OH)_2$) compound which exhibit as UV light absorber. The percentage yields obtained from the hydrothermal extraction consist of 41.2 ± 0.66 % (w/w) of HAp which was almost half of the dry weight of 100 g samples. The additional of manganese and ferum, initiated the novel sunscreen materials from hydroxyapatite-Fe and hydroxyapatite-Mn doped (modified bones). The unmodified HAp recorded with SPF 20 and modified HAp-Mn measured with SPF 40. Modified HAp-Fe emulsions were recorded with SPF 50 as the highest SPF value. Therefore, the bones have been characterized using nuclear magnetic resonance (NMR) spectroscopy and x-Ray diffraction (XRD) and UV-Visible spectroscopy. The results obtained clearly indicated that the HAp existence in waste of *Fringescale sardinella* bones with addition of $FeCl_2$ which exhibits high potential as sunscreen compared to manganese and unmodified bones. Thus, the utilization of waste from the fish bones not only produce value-added products from low-cost resources, but also help in reducing pollution to the environment and preserved the global sustainability.

Keywords: Hydroxyapatite (HAp), Hybrid sunscreen, *Fringescale sardinella*, Crystallite, Utilization fish waste

How to cite this:

Rozaini MZH, Hamzah H, Razali MH, Osman UM, Wai CP, Soh SKC, Ghazali SR, Ibrahim NH and Fei LC, 2019. Diversity and marine sustainability of Setiu wetland: modified calcium phosphate from Tamban bones as alternative sunscreen materials. Asian J. Agric. Biol. Special Issue: 33-47.

Introduction

Tamban sisik (*Fringescale sardinella)* is a type of warm water fish species which belongs to the genus Macruronus and is a member of Merlucciidae family. This fast-growing species constitutes Terengganu's

largest commercial fishery. Tamban sisik is distributed throughout the east coast of peninsular Malaysia. Being able to live more than 10 years and grow to a length of approximately 100 cm, it prefers deep warm water with a depth of 50 m to over 150 m. In appearance, Tamban sisik has a short wedge-shaped body, with slim fins and a blue-green to silver colour pattern Its thick white flesh is high in omega-3 fatty acids, making it a good dietary choice and is currently being used in the production of a variety of consumer products such as fish crackers (Rozaini et al., 2017).

Fishbone is consisting of calcium and phosphate derived by the denaturation of its skeletal and water insoluble fibrous. The toxicity of conventional sunscreen agent: oxybenzone and octinoxate that can disrupt the hormone and skin allergy has open the way for fishbone to be used as a potential substitute. It also meets the requirements of Muslims who consume Halal resources (Rozaini et al., 2017). Fish waste, including skins, bones and scales can be as much as 75% of the initial raw materials. It is occasionally converted to other low-value products or just being discarded into the sea (Kim and Mendis, 2006).

In Malaysia, sunscreen becomes a necessary product among human to protect from hazardous ultraviolet (UV) due to the hot and extremely weather changed. It is known that longer UV exposure can cause sunburns and severe effects (Piccirillo et al., 2013). Sunscreen can be defined as substance that protect the skin from the deleterious UV-light and avoiding or minimizing the damage that radiation may cause from radiation on human health (Salvador and Chisvert, 2005). The UV light composed of three regions which are UVA (320-400 nm) UVB (290-320 nm) and UVC (200-290 nm). However, UVA and UVB can pose a threat to human according to Piccirillo et al., 2013. If the skin repeated exposed, skin aging and skin cancer could cause damage to human DNA and RNA.

Sunscreen agents for instance TiO_2 and ZnO can potentially be replaced with HAp non toxicity calcium phosphate sources from human and animal bones that effectively absorbs the UV region (Araujo et al., 2010; Piccirillo et al., 2013). HAp is commonly used as a filler or coating on damaged bone and implants in order to promote bone in-growth bone especially in orthopedic, dental, maxillofacial and biomedical applications (Ferraro et al., 2013) and cosmetics (Wang et al., 2013). Bones known as white colour, brittle properties and cheaper source that provided abundance of HAp that can turn into good carriers in sunscreen (Springsteen et al., 1999). It also provides a promising candidate for advanced sunscreen. Furthermore, the UV absorption limit can be tuned to absorb in the desired range from UVB to UVA by simply introducing a doping (Piccirillo et al., 2013).

Iron (Fe) and manganese (Mn) can widen UV range absorption in comparison to TiO_2 and ZnO (Araujo et al., 2010). Therefore, by doping fish bone with proper element can initiate a huge potential of sunscreen agent as novel hybrid biomaterials. It was not only potential candidate for sunscreen, but also helping the local fishing industry especially in Terengganu (East Coast Malaysia) to manage bone waste disposal more wisely, improve their economic status and also preserve the environment. In this paper, the synthesis and characterization of modified HAp *Fringescale sardinella* with Fe and Mn as promising new sunscreen absorbance materials or UV filter were discussed.

Material and Methods

All experiments were conducted in triplicate unless stated otherwise.

Traction of Hydroxyapatite (unmodified HAp)

About 30 kg of *Fringescale sardinella* stock were obtained from SmedQ Enterprise (Kuala Terengganu) in 2014. With average length of 80 – 150 mm, the fish were transported frozen to the laboratory and were kept in a -20 °C freezer prior to their preparation.

The frozen fish were defrosted, and the meat were thawed and cleaned. The cleaned fish were then transferred to container and boiled for 36 hours in 200°C. The adherent tissues such as fat, flesh and scales from the skins were removed. The remaining bones were ran through tap water to remove visible impurities prior being transferred to trays and dried in the furnace at 110°C for 24 hours. The dried fishbones were packed and sealed in 150 x 90 mm snap-lock bags (GLAD, Oneplastic, Malaysia) before being stored at 10°C until further use.

The extraction of unmodified HAp from the prepared fishbones involved washing them intap water, treated with 0.8 M NaCl, followed by soaking in 0.2 M NaOH for five hours at 5°C, rinsed again in tap water and treated with 0.05 M acetic acid (1:10 w/v) for three hours at room temperature. The extraction of HAp was performed in Mili-Q water (Millipore Corporation, Billerica, MA, China) (1:10 w/v) for twelve hours at 40°C in a shaking water bath (Ratek Instruments, Boronia, Victoria, Australia). The bone samples were

centrifuged (Sorvall® RC 285) at 10 000 rpm x 60 minutes at 15°C, filtered with Whatman filter paper (No. 5) (Whatman International Ltd., Kent, UK) and the resultant filtrate was freeze-dried using free zone Plus (Labcoco, MO, Malaysia) equipment.

Synthesize of modified hydroxyapatite: modified HAp-Mn and modified HAp-Fe

The preparation of modified Hap-Mn and Hap-Fe will undergo the same procedure as the unmodified HAp. About 30 kg of *Fringescale sardinella* stock were obtained from SmedQ Enterprise (Kuala Terengganu) with average sizes and handling.

The filtered fish bones were then divided into three beakers containing water, iron chloride (98 %, Merck) and manganese chloride (98 %, Merck) respectively. Each of the sample in the beaker was heated up and maintained at 70°C for three hours with constant stirring. Several drops of 1.0 M of ammonium hydroxide were added into the solution of $FeCl_2$ and $MnCl_2$ to reduce the acidity of solution until the pH was approximately 8.0.

The fish bones were dried again an overnight in oven and calcined at 900°C for three hours in a furnace. The sample was then re-weighed using an analytical balance to detect the potential mass loss from the evaporation process. The calcined bones were converted into powder form by grinding with high-energy ball mill for 15 minutes at 450 rpm.

Percentage yield of hydroxyapatite

The yield of HAp was determined based on a dry weight basis and calculated according to **Equation 1**:

$$Yield\ (Y, \%) = \frac{Dry\ weight\ of\ fishbone\ (g)}{weight\ of\ fishbone\ (g)} x\ 100$$

The average yields were expressed in mean ± standard deviation.

Determination of moisture content of HAp

The moisture content of HAp was evaluated using a vacuum oven method based on the AOAC International (2000) method 90.46. A 2 g sample of Tamban sisik (*Fringescale sardinella*) bones were weighed into a dry petri dish and covered with aluminium foil to avoid spattering under vacuum. It was then placed in a vacuum oven (D-63450 Hanau, Kendro, Germany) at 100°C for five hours. The petri dish was cooled in a desiccator and weighted. The moisture content of the Tamban bone was calculated as a percentage of weight loss of the skins after the drying process. The moisture content was calculated according to Equation 2.

$$Moisturecontent\ (\%) = \frac{W_1 - W_2}{Weight\ of\ Tamban\ bones} x100$$

Where W_1 is the weight of the petri dish and wet Tamban sisik bones before the drying process; and W_2 is the weight of the petri dish and Tamban sisik bones after drying process.

The moisture content was reported as mean ± standard deviation.

Characterization

The components and morphology of the synthesized of *Fringescale sardinella* bones in powder form were identified using hydrogen nuclear magnetic resonance (H^1NMR), X-Ray diffraction spectroscopy (XRD), Fourier transform infrared radiation (FTIR) and Scanning electron microscopy (SEM)**.**

Hydrogen nuclear magnetic resonance (H^1NMR)

In this research, H^1NMR was implemented to determine the presence of single proton spectra in a compound of HAp (5 mg bone powders dissolved in chloroform) using Bruker Avance III 400 spectrometer. Higher solubility will result in less noise of spectra.

X-Ray diffraction (XRD)

XRD was performed using Rigaku MiniFlex II diffractometer with Cu Kα. This test was conducted to signify the phase composition obtained in the compound of HAp, HAp-Fe and HAp-Mn. Each sample was poured and smoothly pressed in the small rectangle shape by the glass slide respectively before analyzed by the machine. Samples then were analyzed with a step of 0.02°, over 2θ and between the range of 10° and 80°.

Fourier transform infrared radiation (FTIR)

In this study, FTIR was used to determine the infrared spectrum of absorption of unmodified Hap and modified Hap-Mn and modified Hap-Fe. Bone powder was prepared by mixing with grinded potassium bromide (KBr) with the 1:6 ratio. The mixture was finely pulverized and put into a compressor. KBr become plastic when subjected to pressure and form a sheet that is transparent in the infrared region. FTIR

analysis of three different sunscreen agents were performed to investigate the structure of HAp molecules, according to the position of peak components identified in a known region. The results obtained from this analysis were expected to provide details on the different secondary structures of compound, mainly bone vibration at different peak components.

Observation of microstructure via scanning electron microscope (SEM)

The morphology of fish bones was determined using SEM. All samples were mounted rigidly on a sample holder called a sample stub. Therefore, samples then were sputter coated with gold to ensure the electron conductivity with the sample tested on a plate. A 3 mm x 3 mm cube of a 6.67% fishbone specimen was taken from the centre of the cylindrical gel. It was fixed with 2.5% (v/v) glutaraldehyde in 0.1 M phosphate buffer (pH 7.3) for one hour. The specimen was rinsed thrice in Mili-Q water and dehydrated in ethanol with ascending concentrations of 30%, 50%, 70% and 90% (v/v) for 10 minutes at each concentration. The specimen was then immersed twice in 100% (v/v) of ethanol for 10 minutes each time. It was transferred to ab E3000 Polaron Series II Critical Point Dryer (Polaron Equipment Ltd., UK) using liquefied carbon dioxide as the transitional fluid. The dried specimen was mounted on a SEM stub, coated with platinum (Pt) using a sputter coater Polaron SC 7640 (Polaron ltd, Newhaven, UK) and observed under SEM (Phillips XL30S, FEG, Netherlands) at an acceleration voltage of 5kV.

Determination of thermal transition at different relative humidity values

Fish bones were equilibrated at different relative humidity values (RH, %) before the analysis of thermal transition by different scanning calorimetry (DSC) was conducted. 5 g samples of unmodified HAp, modified HAp-Mn and modified HAp-Fe and zinc oxides were placed in desiccators filled with saturated salt solutions at the bottom of the containers. Three types of salts used were lithium chloride, magnesium nitrate and sodium chloride to achieve relative humidity values of 11.3%, 52.9 % and 75.3% respectively. The samples were equilibrated for five weeks at room temperature. They were then kept in air tight glass vials and stored at -5°C until further use. The moisture content tests of the equilibrated fish bones were conducted according to the procedures describe in determination of moisture.

The moisture content, as indicated by loss on drying (LOD) in the fish, modified fish were determined by complexometric titration using edetate disodium as titrant. During titration, calcium hydroxide could precipitate and interfere with the visual end-point detection. Auxiliary complexing agent such as ammonium acetate buffer (pH 10) was not sufficient to prevent the precipitation of calcium hydroxide. In addition, the complexing agent interfered with the end-point detection. To prevent this phenomenon, the sample solution should be added with the titrant and neutralized prior the actual titration. The optimal amount of edetate disodium required was 18 mL.

Differential scanning calorimetry (DSC)

Thermal transition analysis was conducted using DSC (DSC Q1000, TA Instruments, DE, USA) following the method of Mohtar et al. (2010), to investigate the temperatures of glass transition and the maximum peak of melting of the fish bones. These properties are crucial in identifying the thermal stability such as freezing, cooling and heating. A 4.7 mg sample of fish bones was accurately weight into an aluminium pan and sealed tightly. The sample was scanned over a range of 90 to 300°C at a rate of 10°C/min with liquid nitrogen as cooling medium. The system was equilibrated at 10°C for five minutes before scanning. An empty pas was used as a reference. The instrument was calibrated with indium sample (T_m = 156.6°C). The absorption or release of heat by the samples correspond to the endo- or exothermic peaks as a function of temperature. TA Instruments Universal Analysis Software (TA Instruments, New Castle, DE, USA) was used to analyze the results.

Preparation of photoprotective emulsion

Bronson & Jacobs supplied olive oil (99%) and Moi Foods Malaysia Sdn. Bhd sponsored Olein oil (99%). All the chemicals were used as received without further purification and analytical grade. In order to prepare photoprotective emulsion of unmodified and modified Tamban sisik bones, water was homogenously mixed with surfactant by manual stirring prior homogenizing in a CKL Multimix homogenizer at 1500 rpm for 15 minutes at 25°C ± 0.1. It was during the latter homogenization that the oil was dripped slowly into the mixture.

For the first part of the work, the compositions of the samples were denoted in volume fraction (Ø) and wt%

as presented in Table 1. Microemulsion of N1, N2, N3 and the olive oil proportion was fixed at 75 wt% and N4 and N5 were recorded with 9 wt% with the same amount of surfactant concentration. Equation 3 denounced the calculated volume fraction of oil (Razali et al., 2017).

$$Ø = m_o/\rho_o/[m_o/\rho_o) + (m_w/\rho_w)]$$

Where m_w/ρ_w and m_o/ρ_o represent the volume of water and oil respectively.

Table-1: Composition of control (N1), unmodified *Fringescale sardinella*/HAp bones (N2), modified HAp-Fe (N4) and modified-Mn doped bones (N3) in microemulsion.

Sample	Photoprotective Agents (gram)	Surfactants (wt%)	Water (wt%)	Olive oil (wt%)	Fraction of oil volume (Ø)
N1	0	2.6	23.0	74.5	0.79
N2	10	5.1	21.0	74.5	0.79
N3	10	7.6	18.0	74.5	0.81
N4	10	8.9	12.9	77.9	0.88
N5	10	9.1	8.9	81.9	0.92

For the second part of the work, the volume fraction of oil was 0.80 and the surfactant concentration was 5 wt%. Microemulsion of photoprotective samples were denoted as N1 (olive oil/Tween 80/water/), N2 (olive oil/Tween 80/water/ unmodified HAp), N3 (Zinc Oxide/olein oil/Tween 80/water), N4 (olein oil/surfactant/water/Modified HAp-Mn) and N5 (Modified HAp-Fe/olein oil/surfactant/water) hereafter.

Sunscreen Analysis

The sunscreen analysis was determined to test the capability as sunscreen by in-vitro method using UV Visible spectrophotometer of UV 1700 Shimadzu. An amount of 1.0 g of each formulated microemulsion samples was weighed and transferred into 100 mL of volumetric flask and then was diluted to the graduated mark with ethanol. The solution was homogenized by ultrasonicator for 5 minutes. The homogenized samples were filtered by filter paper and the first 10 mL of microemulsion was expelled. A 5.0 mL of aliquot was transferred to 50 mL of volumetric flask and diluted to the graduated mark with ethanol. All the aliquot solution then was closed in the vials and were kept under dark condition at 25°C.

Results and Discussion

Physical Analysis

Characterization of hydroxyapatite (HAp)/ unmodified bones

The FTIR spectrum of the HAp crystals hindmost at 600°C calcinations are shown at Fig 1(a). There is no alkyl group emerged on the spectrum thus implying the nonappearance of organic materials residual. The residual-free water was stretched and bent at broad band 3000-3800 cm^{-1}.

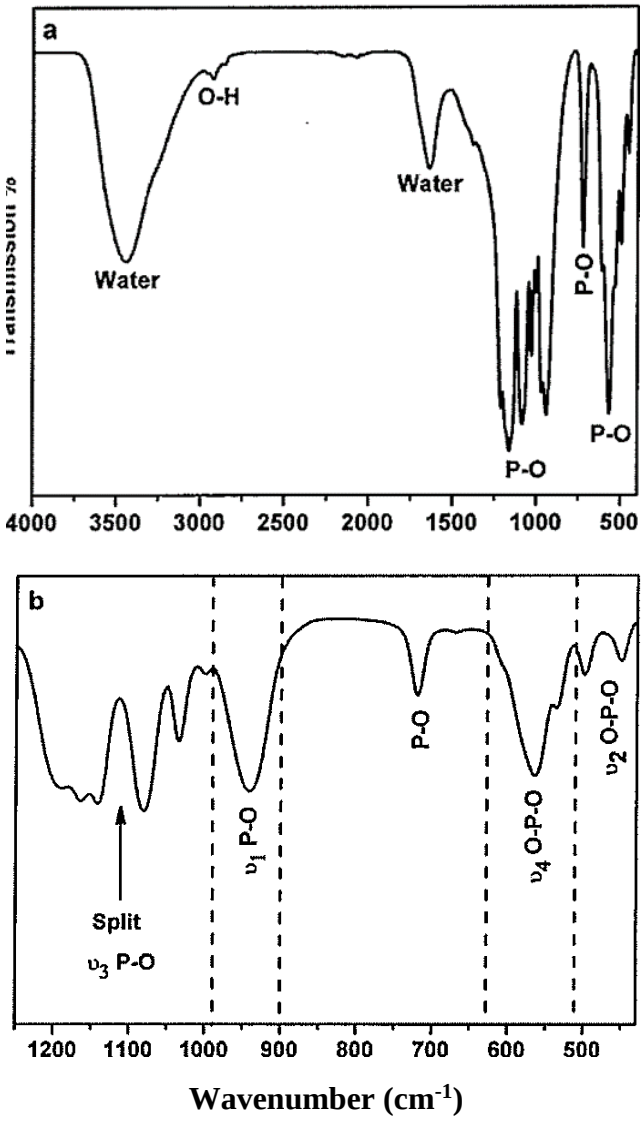

Figure-1: FTIR spectrum of (a) unmodified HAp and (b) highlights of chemical bonding of modified HAp-Fe crystals.

The bending mode of the O-H group by water absorption caused the additional band at 1600 cm^{-1}. The 2900 cm^{-1} feeble band was attributed to the O-H stretching of crystallite (Arifuzzaman and Rohani, 2004). The crystal compounds were highlighted in the FTIR spectrum of Fig 1(b). The spectrum represented PO_4^{3-} were easily differentiate. The phosphate group bending mode (720 cm^{-1}), υ_2 O-P-O bending mode (520-630 cm^{-1}) and υ_4 O-P-O bending mode bands (in the range of 430-520 cm^{-1}) are assigned and comparable to the finding by the Vallet-Regi and Gonzalez-Calbet (2004). Wang et al. (2005) agree with the finding of υ_1 symmetric P-O stretching mode at 900-990 cm^{-1} band and $\upsilon 3$ antisymmetric P-O at 990-1250 cm^{-1} band. The pervasive PO_4^{3-} bands split at 1125 cm^{-1} implies a high degree of crystallinity which is persistent with the XRD result.

The formation of single proton in HAp (δ_H = 1.54) obtained from unmodified HAp derived from *Fringescale sardinella* was confirmed by ^1H spectroscopy (Fig. 2). The effect of dopants on the phase identification of the modified bones, were characterized. Fig. 3 represent the typical XRD patterns of the pure HAp and Fe^{3+}-doped and, Mn^{2+} -doped HAp samples, which perfectly match with the JCPDS pattern #74-566 for HAp. The incorporation of Mn^{2+} and Fe^{3+} into the material apparently leads to the formation of less crystalline HAp. This effect seems natural as the dopants assumed to substitute at Ca^{2+} sites (ionic radius 0.99 Å) have larger charge and smaller ionic radius (Mn^{2+} 0.63 Å, Fe^{3+} 0.64 Å). Several ions, usually with an ionic radius smaller than that of Ca^{2+} are known to inhibit the formation of HAp (Miyaji et al., 2005).

Fig. 3(a) showed the patterns and phase composition of fish bone treated at 900°C. The HAp pictograph showed that 54 % contained of HAp, $Ca_{10}(PO_4)_6(OH)_2$ as the main component. Fig. 3(b) showed the calcium hydrogen phosphate hydroxide, $Ca_9HPO_4(PO_4)_5OH$ as the main phase which contained about 30 % but there is different phosphate-based compound, which contains both iron and calcium - $Ca_9FeH(PO_4)_7$ 21 %. A small amount of alpha hematite, α-Fe_2O_3 and Fe_2O_3 also detected with 28 % and 25 % respectively. This indicates that iron is present with two oxidation states as Fe (II) and Fe (III) in the mixed of phosphate and hematite (Piccirillo et al., 2013).

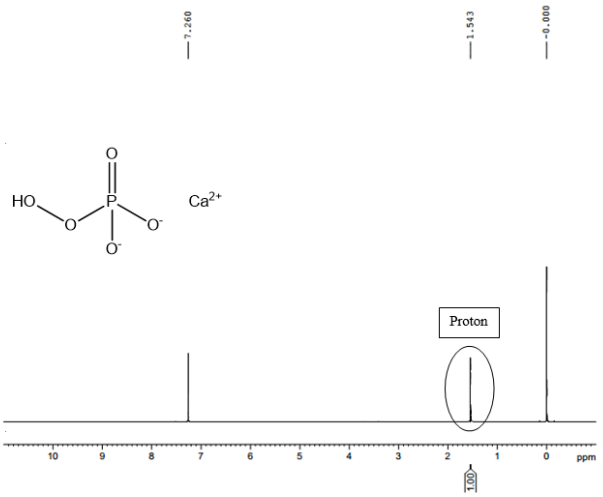

Figure-2: ^1H NMR (400 MHz, $CDCl_3$) analysis of unmodified hydroxyapatite (HAp) derived from *Fringescale sardinella* bones

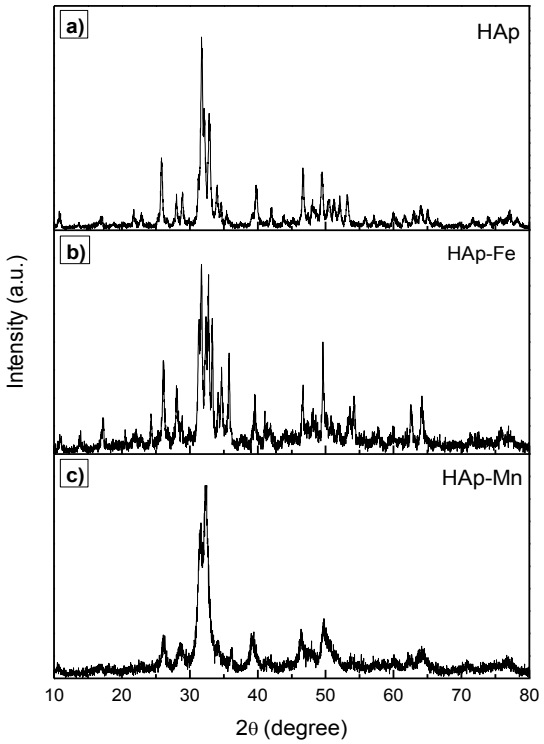

Figure-3: X-ray diffraction pattern of (a) unmodified HAp, (b) modified HAp-Fe and (c) modified HAp-Mn doped compared to the HAp standard pattern PDF #74-566

It can be clearly seen that the colour of modified HAp changed from white into maroon colour during calcinations process. When Mn doped with unmodified bone by mixing with $Mn(NO_3)_2.6H_2O$, two different formula; Chloroapatite, $Ca_5Cl(PO_4)_3$ and $Ca_{10}Cl_2(PO_4)_6$ were obtained as new modified materials. Fig. 3(c) showed that, Mn is still presenting but has been combined with phosphate producing approximately 21 % of manganese chloride phosphate, $Mn_5(PO_4)_3Cl$. Both modified bones resulting in the formation of Fe(III) and Mn (II) in the form of hematite and chloroapatite which help to prevent from UV rays.

The HAp crystals depicted much comparable diffraction profiles and XRD bulk patterns. With the trace amount of HAp, the diffraction peaks of the powders were marked to modified HAp-Fe crystal structure (file no. 2-0085 JCDPDS). There were no detected impurities and no particular peak of other calcium phosphate phases. The samples were well-crystallized reflected by the smooth intensity of the diffraction peaks.

Appearance, moisture and percentage yield

The physical appearance of asynthesize and extraction sunscreen samples are compared in Table 2. Fig. 4 shows the colour appearance of the bones after the calcination process. The unmodified bones were in white ordourless opaque structures (left), the modified HAp-Fe with reddish opaque structures (middle) and modified HAp-Mn with brownish opaque structures (right). Except for colour, all samples generally had similar physical appearances.

Figure-4: The physical appearance of the unmodified (*Fringescale sardinella*/HAp) bones *(left)*, modified HAp-Fe doped *(middle)* and modified HAp-Mn *(right)* after drying and calcination process.

Modified HAp-Fe had the highest content of moisture (10.3 ± 0.13) and pH (7.2 ± 0.32) compared to other samples. The phenomenon observed could be possibly explained by the highest potential of HAp yield initiated during extraction. However, the commercial sunscreen agent, Zinc oxide, (ZnO) had higher moisture content than modified HAp-Mn and unmodified HAp. The pH of pure unmodified HAp is slightly lower than ZnO but not significantly different from that of modified HAp-Mn at P<0.05

Table-2: Physical appearance of the investigated sunscreen agents

Sunscreen Sample	Physical appearance			
	Before drying	After drying	Moisture (%)	pH (1%)
Standard HAp	White odorless powder	White opaque powder	4.6 ± 0.05^{b}	6.3 ± 0.21^{a}
Unmodified HAp	White strong odorous powder	White opaque powder	8.12 ± 0.16^{a}	6.9 ± 0.12^{a}
Modified Hap-Fe	White odorous powder	Reddish odorless powder	10.3 ± 0.13^{a}	7.2 ± 0.32^{b}
Modified Hap-Mn	White odorous powder	Brownish odorless powder	9.16 ± 0.03^{b}	7.1 ± 0.22^{b}
Zinc Oxide, (ZnO)	Yellow odorless powder	Yellowish odorless powder	9.19 ± 0.1^{b}	7.5 ± 0.23^{a}

Values are the mean ± standard deviation of triplicate samples

[a-b] Means with the same superscript within a row are not significantly different (P<0.05)

Table-3: Yield, melting point and viscosity of synthesize sunscreen samples.

	Yield (%)	Melting Point (°C)	Viscosity (Pa)
Commercial Hydroxyapatite	NA	16.2	9.1
Unmodified HAp	41.2 ± 0.66[b]	18.6 ± 0.42[a]	18.8 ± 0.55[a]
Modified HAp-Fe	NA	26.9 ± 0.65[a]	20.8 ± 0.65[b]
Modified HAp-Mn	NA	29.1 ± 0.26[c]	19.0 ± 0.26[b]

Values are the mean ± standard deviation of triplicate samples

[a-b] Means with the same superscript within a row are not significantly different ($P<0.05$)

Yield (weight of hydroxyapatite per 100 g of dry Unmodified Tamban bones)

NA: Not Applicable

The result of the unmodified HAp yield extracted was expressed as a percentage (%) on a dry weight basis. From Table 3, the yields obtained from the extraction consist of 41.2 ± 0.66 % (w/w) which was almost half of the dry weight of 100 g samples. With the moisture content of 9.6, this is more likely a maximum yield can be obtained. This also may be due to the mild conditions used in the extraction of unmodified HAp, which involved a moderate concentration of NaCl solution during the pre-treatment and low temperature for hot water extraction.

The total calcium content in all bones, determined by complexometric titration, varied from 28- 32% w/w with the percentage relative of standard deviations (RSD) round 0.1 – 0.7 (n = 3) (Table 4). These finding are comparable with Kim *et al.*, (1998), which recorded the range of 30.1 – 35.6 % w/w of various fishes including cod, Alaska Pollack, yellowfin sole, hoki, conger ell and mackerel. In comparison, calcium content in *Fringescale sardinella* bones emerged as the highest value with 35.4% and agreed with finding by Rozaini et al. (2017) which recorded the calcium value of 35.6 – 36.3 % for *Sardinella fimbrata* species. Nonetheless, the calcium content may differ based on feed nutrition, species and age.

Unmodified HAp bone had a melting point range of between 17 to 19°C, while that for modified HAp-Fe and modified HAp-Mn were 26 to 27.5°C and 28.5 to 30°C respectively: significantly different from each other at $P<0.05$ (Table 4). The results obtained in this study were consistent with the finding of Miura et al. (2012) who found that an increased in compound strength is accompanied by an increase in melting point. Modified HAp-Fe and modified HAp-Mn have considerably higher melting points than originally unmodified HAp because of the metal involved as inorganic substances needed extra energy to be broken down. However, the melting point of Unmodified *Fringescale sardinella* bones obtained in this study was higher than the one reported by Piccirillo et al. (2013) using Cod Fish bones of cold-water fish taken from northern Atlantic Ocean.

Table-4: Total calcium content in the investigated HAp samples.

	% RSD	% Calcium content
$Ca_5(PO_4)_3(OH)$ Sample	**< 2**	**98.0 – 100.5 $Ca_5(PO_4)_3(OH)$**
Unmodified HAp	12.7	35.4 (0.7)
Modified HAp-Fe	12.0	33.8 (0.7)
Modified HAp-Mn	11.8	31.2 (0.6)
Tamban Beluru (*Sardinella fimbrata*)	12.2	36.3 (0.7)
Giant seaperch (*Lates calcarifer)*	11.5	28.3 (0.1)*
Hoki (*Macruronus novaezelandiae*)	12.5	31.8 (0.7)*

**Obtained from Mokhtar (2013)*

Determination of thermal transition

Thermal transition is an important physical parameter in industrial application because it describes the physical and chemical behavior of the compound systems. It is used to define the thermal transitions involved in the changes in heat capacity, such as melting, glass transition, recrystallisation, entropy and enthalpy, endothermic and exothermic decompositions of various materials with pronounced sensitivity (Mohtar et al., 2010). Differential scanning calorimetry (DSC) thermogram is a representation of the heat flow as a function of temperature. Any changes in specific heat produced in response to the heat flow through the material will show as exothermic or endothermic peaks in the individual thermogram (Turgeon et al., 1996). The area under the curve is proportional to the total enthalpic change. Glass transition has been observed in several cosmetic applications such as in the crystallization of sucrose in amorphous solids, changes in textural properties of emulsion and the non-enzymatic rates of glucose and glycine.

Therefore, the thermal transition of unmodified HAp, modified HAp-Fe and modified HAp-Mn equilibrated at 11.3%, 75.3% and 52.9% were performed using DSC to examine their thermal properties. The thermal properties of sunscreen, which involved the temperature of glass transition (Tg) and the peak temperature of melting are given in Table 5. The

results showed a trend of higher moisture content with increased relative humidity values. This observation could possibly be explained by the presence of a much greater content of calcium ion in unmodified HAp bone than in modified one. This finding is consistent with the current results obtained from the humidity analysis, which demonstrated that the modified HAp-Fe contained a much higher level of moisture content compared to unmodified HAp and modified HAp-Mn. As expected, the glass transition temperatures (T_g) for all sunscreen samples were progressively lowered with increasing relative humidity values (Table 5). Unmodified HAp had an initial temperature of 19°C and decreased to -24°C with an increased in relative humidity from 11.3% to 52.9%. However, the temperature decreased when the sunscreen was equilibrated at the highest relative humidity of 75.3% (-11°C). Such decreased could be explained by the occurrence of ionic compound and metal molecules, while the increased in temperature may be described the absorption properties of the sunscreen. The presence of water as a plasticizer in the sunscreen has decreased the glass transition temperatures and resulted in its structural changes with hydration. This observation may suggest that the effect of absorbed water on sunscreen from different sources varied depending on the differences in their molecular structures. This fact is supported by the finding of Uppgard (2002) who postulated the formation of brown pigment in amorphous solids was largely affected by their thermal properties.

A comparable trend of glass transition temperatures was also observed in the case of modified *Fringescale sardinella* bones-ferum and *Fringescale sardinella* bones-manganese. However, these modified exhibited much higher temperature than the original bones that equilibrated at 11.3%. 52.9% and 75.3% were 90°C, 40°C and 20°C, respectively. The peak melting temperature increased with an increase in relative humidity up to 52.9%; however, the temperature decreased at the highest moisture content (relative humidity value of 75.3%) as given in Table 5. Note that the transition temperature, T_g (mid) and T_g (end) of all bones also appeared to decrease with the increased in moisture content (Table 5), following the trend of initial glass transition (T_g initial) discussed above. The transition temperatures of all bones were significantly different to each other, indication the complexity of the hydration that contributed to the difference in glass transition. This fact is in agreement with Kim et al. (1998), who, working with fish bones as food products, describes the variation of glass transition as possibly due to the different extraction conditions and intrinsic characteristics of the raw materials.

Table-5: Physical properties of synthesize sunscreen samples.

	RH (%)	Moisture (%)	T_g (Init, °C)	T_g (mid, °C)	T_g (end, °C)	T_m (peak, °C)
Unmodified HAp	11.3	5.2	19	32	45	150
	52.9	9.5	-24	-8	2	170
	75.3	10.9	-11	-10	-1	151
Modified HAp-Fe	11.3	7.7	60	71	84	140
	52.9	8.6	52	59	65	157
	75.3	10.4	40	53	60	120
Modified HAp-Mn	11.3	6.1	71	75	90	167
	52.9	8.4	34	39	51	170
	75.3	10.3	30	41	57	149

RH: Relative humidity (%), Moisture: moisture content of equilibrated sunscreen (%), T_g (initial): Initial glass transition, T_g (mid): Mid glass transition, T_g (end): End glass transition, T_m (peak): Peak temperature of melting. Values are the mean of triplicate samples

Observation of the microstructure

The microstructure of three bone samples were determined by optical microscope to observe their structural differences. Fig. 5 shows the images of unmodified HAp, modified HAp-Fe and modified HAp-Mn observations captured at 10,000x magnification. Fig. 5(a) showed the unmodified HAp which exhibited loosen structural properties to that modified HAp-Fe and modified HAp-Mn. It also showed the presence of Ca^{2+} strands with fewer interconnections and larger pores in the system (pointing up by the arrow). Indicating a relatively weak intercalating network.

The modified HAp exhibited superior structural properties compared to unmodified and their microstructures were relatively small to each other (indicated by the arrows). A compact calcium structure and many small pores were observed in the modified HAp-Mn on Fig. 5(b). This has led to a noticeable compaction of the network structure, corresponding with a high strand value of Manganese metal chelation structures.

The modified HAp-Fe exhibited a more compact structure of networks compared to those observed in the unmodified HAp and modified HAp-Mn. It also exhibited a much greater number of interconnected

small pores than the modified HAp-Mn (indicated by the arrows shown in Fig. 5(c) This phenomenon is supported by Kim et al. (1998) who reported on the structure from Cod fish bone and postulated that a higher number of small interconnected pores lead to a stronger powder network. The difference in the microstructure of sunscreen could also be due to different extraction conditions applied during the manufacturing process.

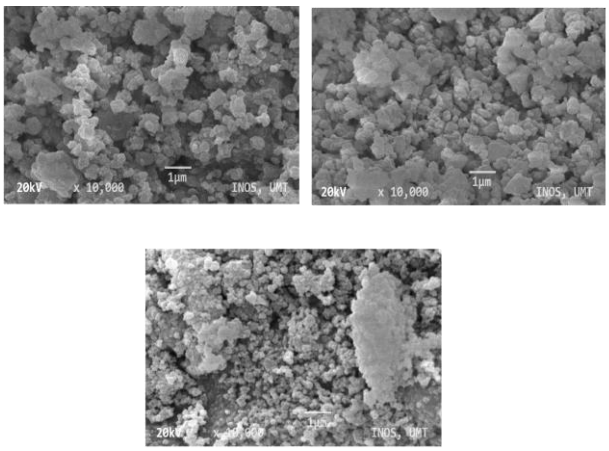

Figure-5: Microstructure observation on (a) unmodified HAp, (b) modified HAp-Mn doped and (c) modified HAp-Fe doped using SEM with 10,000x magnification.

From the optical images, it is clear that the structural differences observed in all sunscreens contributed to the differences in their properties, especially in the strand and metal content. The results also positively emphasized that the microstructures of sunscreen were highly affected by their properties arrangement, in which denser strands (exhibited by the modified HAp) represented higher compound strength than did the looser strands present in unmodified HAp.

Mn^{2+}-doped HAp can be obtained without producing significant alterations in the structure of HAp. On the other hand, Le Geros et al. (1989) reported that incorporation of reduced amounts of Mn^{2+} into HAp structure induces an evident reduction of the degree of crystallinity of the HAp phase. Modified HAp-Fe exhibited high crystalline peak of reduced amounts of Fe^{3+} into HAp structure induces an evident reduction of the degree of crystallinity of the HAp phase. In this work, modified HAp-Fe doped exhibited high crystalline peak at about 33.11°; almost identical to the patterns that were recorded for pure and doped powders. The relatively broadening of the XRD peaks for Fe^{3+}-doped HAp indicates that the sizes of the crystallite grains of those materials are smaller than the pure HAp and modified HAp-Mn. Through Scherrer's equation, the medium crystallite sizes were estimated. The Scherrer's equation, in X-ray diffraction and crystallography, is a formula that relates the size of sub-micrometre particles, or crystallites, in a solid to the broadening of a peak in a diffraction pattern. It is used in the determination of size of particles of crystals in the form of powder. The Scherrer's equation can be written as:

$$\tau = K\lambda / B\cos\Theta \quad \textbf{Eq. 4}$$

Where τ is the mean size of the ordered (crystalline) domains, which may be smaller or equal to the grain size. K is a dimensionless shape factor, with a value close to unity. The shape factor has a typical value of about 0.9, but varies with the actual shape of the crystallite. λ is the X-ray wavelength. β is the line broadening at half the maximum intensity (FWHM), after subtracting the instrumental line broadening, in radians. This quantity is also sometimes denoted as $\Delta(2\theta)$ and θ is the Bragg angle (in degrees).

Table-6: Medium size crystallite obtained via XRD measurements using Scherer's equation to HAp prepared with different dopant at room temperature

Sample	Crystallite size ± 1 (nm)
Pure HAP	27
Modified HAp -Mn	23
Modified HAp -Fe^{3+}	25

Note that the effect of Mn^{2+} on the growth of HAp particles is more remarkable than Fe^{3+}, although the reason for this difference remains unclear at the present crystallite size as shown on Table 6.

The attachment with HAp in nano size has been modified, exploring its absorption capability and its intense dispersing of the solar radiation in the UV region. The sunscreen or photoprotection action of that material the method of diffuse reflectance was applied. Titanium dioxide (TiO_2) was performed as measurements of reflectance which commonly used in sunscreens formulations especially in cosmetics industry. Furthermore, TiO_2 is an inorganic UV filter in sunscreen products to protect the skin from harmful UV rays when exposed to sunlight (Razali et al., 2017). In Fig. 6, TiO_2 showed one large absorption around 268-419 nm can be seen.

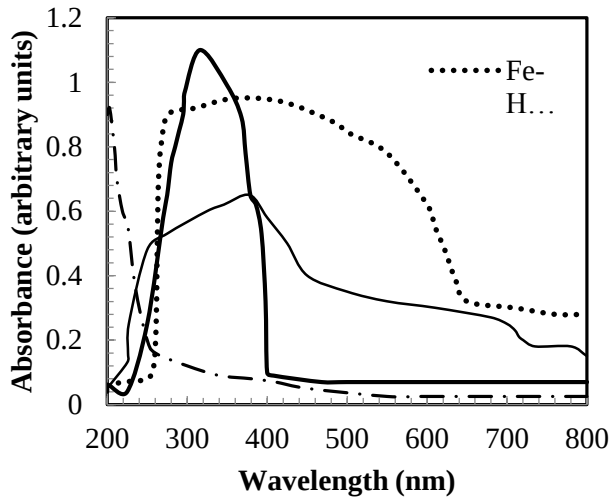

Figure-6: Comparison UV-Vis absorption spectra of TiO_2, pure HAp, Mn^{2+}, Fe^{3+}-doped HAp

Widely used TiO_2 is also semiconductor that can absorb light and under certain conditions generates free radicals. The minimum energy of TiO_2 required to excite an electron from its valence band to its conduction band is 3 eV (Brezova and Stasko, 1994). Basically, compound with this kind of band gap can be promoted by radiation at wavelengths below than 380 nm. Thus, TiO_2 may be vulnerable to excitation of electron by UVB and UVA in sunlight. TiO_2 also could promote a single electron from the valence band to the conduction band by photoexcitation and leaving a positively charged space that also known as a hole behind (Rozaini et al., 2017). Normally, the electron reunites with the hole, but sometimes the hole migrates to the particle surface, where it can react with absorbed species. It can react with water or hydroxyl ions and forming hydroxyl radicals in an aqueous environment (Razali et al., 2017). For aqueous preparations of TiO_2 is widely known such reactions, exposed to either artificial UV light or natural sunlight. At this stage, the photocatalytic potential of TiO_2 has been utilized to break down suspensions of organic materials and purify drinking water experimentally.

Zinc oxide was found that prevents and block mostly UVA radiation and has an attenuation maximum around 380 nm, but this can differ slightly with particle size (Pinell et al., 2008). It also has been clearly shown to be similar to that of TiO_2 based on photocatalytic mechanism (Dindar and Icli, 2001; Rozaini and Brimblecombe, 2009). Food and Drug Administration (FDA) in 1993 has clarified that a sunscreen or photoprotective should maintain wavelength of UVA around 360 nm to declare to be anti-UVA and the material used in the formulation should be able to present absorption in this spectrum region (Piccirillo et al., 2013)

The spectra of pure, modified HAp-Mn and modified HAp-Fe produced by UV–Vis absorption is shown in Fig. 6 and the Table 7 is presented the maximum absorption wavelengths for TiO_2, pure and –doped attached with HAp. UV region around 200-340 nm with a strong band below 247 nm shows optical absorption in pure HAp. Results for producing pure HAp by an aqueous precipitation procedure from $Ca(OH)_2$ and H_3PO_4 at temperature 900 ^{0}C similarly were found by Nishikawa (2001).

Table-7: Maximum absorption wavelengths of the powders

Powders	Maximum Absorption (nm)
Pure	207
Mn^{2+}	240-372
Fe^{3+}	310 - 427
TiO_2	316

The optical absorption of HAp had undergone remarkable changes with the introduction of Fe^{3+} and Mn^{2+} as can be seen in Fig. 6. Mn^{2+}-doped HAp generates absorption bands from UV to the visible (250 – 380, 450 – 700, 730 - 800 nm). Fe^{3+}-doped HAp showed a broaden absorption from UV to the visible (267-650 nm) regions. The possibility of an unacceptable visual color effect in sunscreens can produce by absorption bands in the visible region. To prevent the agglomeration of particles, care has to be taken during sunscreen production, because the final effect of the product will decrease, and the bad dispersion will yield a colored film. Thus, this problem can be work out if there is a better dispersion of the sunscreen on the skin and a colored sunscreen will have transparent appearance when correctly applied on the skin (Flor and Davolos, 2007). The Fe^{3+}-doped HAp is the best sample because it showed absorption features in the wider spectral interval of 213-650 nm, which is similar obtained for TiO_2 even if the Mn^{2+}-doped HAp had good results in their absorption spectrum. Moreover, it is known that a highlighted sunscreen should have maximum absorption capacity in relationship the UV radiations in wavelengths between 296.7 and 700 nm Substances with higher absorbance embraced the highly UV absorbance potential (Harry, 2003). Undoubtedly, the most promising sample produced in this work is the Fe^{3+}-

doped HAp with this aim.

Sun protection factor (SPF) for unmodified HAp and modified HAp-Fe and HAp-Mn

The measurement of UV-vis absorption spectra has been made to the unmodified and also modified *Fringescale sardinella* bones with the comparative study of the SPF measurement among photoprotective emulsions (sunblock or sunscreen) available on the market and sold commercially. This can make an accurate comparison to the extent of photoprotective agents that have been used as active ingredients and verification of the SPF.

The increase in the SPF value indicates higher UV protection. Thus, measuring SPF value allow us to know the efficiency of formulation to protect skin from aging, cancer, sunburn and other skin damage (Omar and Abdulrahman, 2015). In fact, sunscreens with sufficient SPF values are used to support the body's natural protection mechanisms to protect against injurious UV rays through absorbing, reflecting or scattering the sun's radiation (Mbanga et al., 2014).

All microemulsion formulations were stable after four weeks of storage. The appearance was white and creamy yellowish in color for N1 and milky white in color for the rest. At the end of storage period, there were no physical changes on formulation samples (Fig.7). The colour differences and appearance of four microemulsion formulation samples as stated in Table 8 with the combinations of different active ingredients or photoprotective agents (unmodified and modified bones) along with non-ionic surfactants (i.e. Span 20, Span 80, Tween 20 and Tween 80) with olive oil (co-surfactant) and water.

Figure-7: Appearance of control (N1), unmodified *Fringescale sardinella*/HAp bones (N2), modified HAp-Fe (N4) and modified-Mn doped bones (N3) in microemulsion.

Table-8: Sun protection factor (SPF) value of the sunscreen formulation

Formulation	Active Ingredients	Amount (%)	Sunscreen Protection Factor (SPF)
N1	0	0	9.630 ± 1.5
N2	unmodified HAp	3.0	23.533 ± 1.3
N4	modified HAp-Fe	3.0	48.940 ± 1.2
N3	modified HAp-Mn	3.0	40.469 ± 1.6

All values are presented as Mean ± SD (*n* =3)

Table-9: Absorbance values of the sunscreen formulation

Wavelength (nm)	Formulation 1 (N1)	Formulation 2 (N2)	Formulation 3 (N3)	Formulation 4 (N4)
290	2.497	4.708	5.685	6.411
295	2.131	4.539	5.195	6.174
300	1.819	3.194	3.883	4.854
305	1.613	1.916	3.662	4.300
310	1.459	1.380	3.506	4.126
315	1.284	1.110	3.351	3.720
320	0.828	0.859	1.739	3.364

The SPF values were in the range of 1 to 50 (Table 8). Formulation 4 had a high calculated SPF value with 48.940 ± 1.2, and in close arrangement with the marketed sunscreen product labeled with SPF value 50. The values were calculated using the absorbance value from the UV spectrophotometer measurements as shown as Table 9. Control sample of formulation 1 (consist of microemulsion without active ingredients of photoprotective substances) had the lowest calculated SPF value compared to the other formulations in this analysis and was labeled as SPF 10.

Furthermore, formulation 2 had a SPF value of 23.553 ± 1.3. As can be observed, the calculated SPF value for formulation 2 is 1.275x different compared to the commercially sunscreen product with the label SPF 20 and even larger difference when compared to formulation 4. Formulation 3 can be labeled as SPF 40 while formulation 4 can be considered as sunscreen with SPF 50. The reason for this variation and difference in calculated SPF value might be due to the metal interaction of vehicle components and concentration of sunscreen formulations (Hernandez and Goymann, 2006)

Among the four formulation samples analyzed, it showed that formulation with surfactant, especially formulation 4 containing modified HAp-Fe doped showed better maximal absorbance values and have the potential as the best sunscreen formulation compared to the other formulations. The good stability

of composition from its components and the combination in its formulation might resulted in a higher calculated SPF value for formulation 4. About 3% modified HAp-Fe content was chosen, even though the maximum amount of photoprotective capacities were allowed is until 20%. Hence, according to *Boot Star Rating* classification system, developed by *Boots*, one of UK's main sunscreen manufacturers and sellers, these microemulsion offering the maximum UVA protection and would be rated as 5 stars.

Further in depth discussing, it is unquestionable that the SPF value affected the efficacy of a sunscreen formulation. As the UV spectrophotometric technique involves low-cost reagents, rapid, and simple, it is the most recommended analysis to determine SPF values *in vitro* as discussed thoroughly by groups of researchers (Mansur et al., 2010).

In addition, Mansur et al. (2010) established a simple mathematical equation which substitutes the *in vitro* method proposed by Sayre et al. (2009) and it is very useful in the calculation of SPF value for sunscreen formulation. Moreover, the proposed methodology also can be suggested as an easy and convenient technique to monitor the quality during production of sunscreens. Consequently, this method can be used in the SPF determination of any organic and inorganic sunscreen formulations.

Basically, according to Prasanna et al. (2015), SPF values in the sunscreen's formulation can be affected by many factors, including solvents used during production, emulsion types and the interactions of vehicle components (e.g. emollients and emulsifiers) within the formulation, and the combination and concentration of the sunscreen compound. Besides that, the UV absorption of each sunscreen formulation is also affected by the addition of other active ingredients, the viscosity, pH system, and the rheological properties (Dutra et al., 2004).

In turn, with the increase in people's awareness of the detrimental effect from UV radiation, this analysis serves as one of the important findings in terms of skin protection by using a sunscreen product based on marine extract. The development of an ideal biomaterial of HAp derived from Tamban bone as sunscreen formulation with a better safety, non-irritating, non-toxic and also photostable is necessary in facilitating the decrease of the negative impact of UV rays on skin. In terms of the photoprotection properties, all of the samples formulations in this study exhibited different calculated SPF values greater than SPF 20 (except for F1 as control). Data variation of those formulations could be due to their composition of their active ingredients of photoprotective substances and also the micro emulsified system. Formulation F4 with 3% of modified HAp-Fe content may be too high in the emulsion to embed itself properly into the structure of the cream with mixing achieved at room temperature. The significant effect on the UV-Vis properties may be affected by subsequent homogenization process. The more homogeneous and enhanced mixture was obtained between the powder of Tamban-modified and the microemulsion.

Conclusion

This research has proved the concept of innovating waste to wealth. Local resources have been explored thoroughly in order to create something very useful to community along with the smartest way on utilize the waste. Tamban (*Fringescale sardinella*) bones collected from factory waste are currently emerged as a potential and promising application for the sunscreen formulation in cosmetics. This study investigated the role of HAp derived from Tamban bone and the modification of unmodified HAp with the ferum and manganese doped in microemulsion structure, which was used as a reaction medium for the synthesis of novel sunscreen agents. The percentage yields obtained from the extraction consist of 41.2 ± 0.66 % (w/w) which was almost half of the dry weight of 100 g bone samples. Pure HAp (unmodified Tamban bone) recorded with SPF 20 and modified HAp-Mn doped measured with SPF 30. Modified HAp-Fe microemulsions were recorded with SPF 50 and the highest SPF value. Ten over-the-shelf sunscreen products with an SPF range of 10-50 were also tested. The SPF values of the 30% of the analyzed samples were in close agreement with the labelled SPF, 30% presented SPF values above the labelled amount and 40% presented SPF values below the labelled amount. This is really a good indicator where we can synthesize more metal doping into HAp to increase their absorbance as well as SPF values.

Acknowledgement

We thank our colleagues Mr Nasrul Yahya from Technology Park Malaysia, Raub who provided insight and expertise that greatly assisted the research,

with all of the interpretations of this paper and also to all volunteers who made this investigation possible.

Contribution of Authors

Rozaini MZH: Conducted the study and prepared the manuscript draft
Hamzah H: Data collection and manuscript writing
Razali MH: Data interpretation
Osman UM: Data interpretation
Wai CP: Data interpretation
Soh SKC: Structural and Statistical analysis
Ghazali SR: Data collection and manuscript writing
Ibrahim NH: Supervised the study and prepared the manuscript draft
Fei LC: Manuscript final reading & approval

Disclaimer: None.
Conflict of Interest: None.
Source of Funding: Niche Research Grant Scheme NRGS 53131/SG01/2016, Fundamental Research Grant Scheme initiative (via FRGS 59423/SG01/2017) and Prototype Research Grant Scheme (via PRGS 54251/SG01/2019)

References

Araujo TS, Souza SO, Sousa EMB and Araújo MS, 2010. Production and thermal stability of pure and Fe^{3+} - doped Hydroxyapatite. J. Phys. Conf. Ser. 249: 1-7.

Arifuzzaman SM and Rohani S, 2004. Experimental study of brushite precipitation. J. Cryst. Growth. 267: 624-634.

Brezova V and Stasko A, 1994. Spin trap study of hydroxyl radicals dormed in the photocatalytic system TiO_2-water-p-ceesol-oxygen. J. Cat. 147: 156-162.

Dindar B and Icli S, 2011.Unusual photoreactivity of zinc oxide irradiated by concentrated sunlight. J. Photochem. Photobiol. A: Chem. 140:263-268.

Dutra EA, Oliveira DA, Kedor-Hackmann ER and Santoro MI, 2004. Determination of sun protection factor (SPF) of sunscreens by ultraviolet spectrophotometry. Revista Brasileira de Ciências Farmacêuticas. 40(3): 381–385.

Ferraro V, Carvlho AP, Santos MM, Castro PML and Pintado ME, 2013. Extraction of high added value biological compounds from sardine, sardine-type fish and mackerel canning residues - A review. Mat. Sci. Eng: C. 33: 3111–3120.

Flor J and Davolos MR, 2007. UVA I-protection effectiveness of bioactive compound and organic UV filters: an *in vitro* assessment. Quimica. Nova. 32:5-10.

Harry RG, 2003. Harry's cosmeticology. 13th edition. Leonard Hill Books, London, UK.

Hernandez JR and Goymann CCM, 2006. Sun protection enhancement of titanium dioxide crystals by the use of carnauba wax nanoparticles: The synergistic interaction between organic and inorganic sunscreens at nanoscale. Int. J. Pharm. 322:161-170.

Kim JM, Vanguri S, Boeke JD, Gabriel A and Voytas DF, 1998. Transposable elements and genome organization: comprehensive survey of retrotransposons revealed by the complete. Saccharomyces cerevisiae genome sequence. Genome Res. 8(5): 464-78.

Kim SK and Mendis E, 2006. Bioactive compounds from marine processing by products –A review. Food Res. Int. 39(4): 383-393

Le Geros RZ, Taheri MM, Quirologico GB and Le Geros JP, 1989. Proceeding of 2nd International Phosphorus Conference, Boston, USA. pp. 89-103.

Mansur JS, Breder MNR, Mansur MCA and Azulay RD, 2010. Determinacão do fator de protecão solar por espectrofotometria. An. Bras. Dermatol. Rio de Jenairo. 61: 121-124.

Mbanga L, Mulenga M, Mpiana PT, Bokolo K, Mumbwa M and Mvingu K, 2014. Determination of Sun Protection Factor (SPF) of some body creams and lotions marketed in Kinshasa by Ultraviolet Spectrophotometry. Int. J. Adv. Res. Chem. Sci. 1(8): 7–13.

Miyaji F, Kono Y and Suyama Y, 2005. Formation and structure of zinc-substituted calcium hydroxyapatite. Mat. Res. Bull. 40: 209-220.

Miura T, Yamana Y, Usui T, Ogawa H, Yamamoto M and Kusano K, 2012. Homologous recombination via synthesis-dependant strand annealing in yeast requires the Irc20 and Srs DNA helicases. Genetics. 191(1): 65-78.

Mohtar NF, Perera C and Quek SY, 2010. Optimisation Of gelatine extraction from hoki (*Macruronus novaezelandiae*) skins and measurement of gel strength and SDS-PAGE. Food Chem. 122: 307-313.

Nishikawa H, 2001. Thermal behavior of hydroxyapatite in structural and spectrophotometric characteristic. Mat. Lett. 50 (5): 364-370.

Omar KA and Abdulrahman RS, 2015. Determinations of sun protection factor (SPF) of some sunscreens marketed in Kurdistan region by UV-visible spectrometry and study their rheological properties. Int. J. Pharm. Chem. 5(2): 40–44.

Prasanna KTP, Prakash NKS, Lokesh P and Manral K, 2015. A simple and rapid method developed to determine the Sun protection factor (SPF) by using UV-visible spectrophotometer for topical formulations. J. Res. Method. Edu. 5 (1): 1–5.

Piccirillo C, Silva MF, Pullar RC, Braga da Cruz I, Jorge R, Pintado MM and Castro PM, 2013. Extraction and characterisation of apatite- and tricalcium phosphate-based materials from cod fish bones. Mater. Sci. Eng. C. Mater. Biol. Appl. 33(1): 103-110.

Razali MH, Osman UM, Rozaini MZH and Yusoff M, 2017. Thermal Stability on Morphology and Crystal Structures of Hydrothermally Synthesized Titanate Nanotubes and Their Photocatalytic Activity. Asian J. Chem. 29(10). 2207-2210.

Rozaini MZH and Brimblecombe P, 2009. The odd-even behaviour of dicarboxylic acids solubility in the atmospheric aerosols. Water Air Soil Pollut. 198: 65-75.

Rozaini MZH, Hamzah H, Mohtar NF, Sainoruddin MH, Fakhrul Sofian FR, Ghazali MS, Wahid ME, Ghazali SR and Razali MH, 2017. Novel materials derived from *Sardinella fimbriata* (Tamban) bones as anodyne sunscreen: towards zero fisheries waste for global sustainability. J. Sustain. Sci. Manag. NRGS Special Issue. 3:75-84.

Sayre RM, Agin PP, Levee GJ and Marlowe E, 2009. Comparison of *in vivo* and *in vitro* testing of sunscreening formulas. Photochem. Photobiol. 29: 559-566.

Salvador A and Chisvert A, 2005. Sunscreen analysis a critical survey on UV filters determination. Anal. Chim. Acta. 537(1-2): 1-14.

Springsteen A, Yurek R, Frazier M and Carr KF, 1999. In vitro measurement of sun protection factor of sunscreen by diffuse transmittance. Anal. Chim. Acta. 380:155-164.

Turgeon SL, Sanchez C, Gauthier SF and Paquin P, 1996. Stability and rheological properties of salad dressing containing peptidic fractions of whey protein. Int. Dairy J. 6: 645-658.

Uppgard F, 2002. The historical aspects of sunscreens. J. Photochem. Photobiol. B: Biol. 64(2-3): 99–104.

Vallet-Regi M and Gonzalez-Calbet JM, 2004. Calcium phosphates as substitution of bone tissues. Prog. Solid State Chem. 32: 1-31.

Wang C, Chang T, Shi L, Yang H, Cui M and Tambalu L, 2013. Seafood processing by-products: collagen and gelatin. Kim, S.K. (ed.). Trend and Applications. New York: Springer Science.

Wang YJ, Lai C, Wei K and Tang SQ, 2005. Influence of temperature, ripening time, and cosurfactant on solvothermal synthesis of calcium phosphate nanobelts. Mat. Lett. 59: 1098-1104.